PHYSICAL REVIEW D **93,** 123510 (2016)

Weak annihilation cusp inside the dark matter spike about a black hole

Stuart L. Shapiro* and Jessie Shelton

Department of Physics, University of Illinois at Urbana-Champaign, Urbana, Illinois 61801, USA

(Received 28 April 2016; published 7 June 2016)

We reinvestigate the effect of annihilations on the distribution of collisionless dark matter (DM) in a spherical density spike around a massive black hole. We first construct a very simple, pedagogic, analytic model for an isotropic phase space distribution function that accounts for annihilation and reproduces the "weak cusp" found by Vasiliev for DM deep within the spike and away from its boundaries. The DM density in the cusp varies as $r^{-1/2}$ for s-wave annihilation, where r is the distance from the central black hole, and is not a flat "plateau" profile. We then extend this model by incorporating a loss cone that accounts for the capture of DM particles by the hole. The loss cone is implemented by a boundary condition that removes capture orbits, resulting in an anisotropic distribution function. Finally, we evolve an initial spike distribution function by integrating the Boltzmann equation to show how the weak cusp grows and its density decreases with time. We treat two cases, one for s-wave and the other for p-wave DM annihilation, adopting parameters characteristic of the Milky Way nuclear core and typical WIMP models for DM. The cusp density profile for p-wave annihilation is weaker, varying like $\sim r^{-0.34}$, but is still not a flat plateau.

DOI: 10.1103/PhysRevD.93.123510

I. INTRODUCTION

A supermassive black hole (SMBH) will steepen the density profile of dark matter (DM) within the hole's sphere of influence, $r_h = GM/v_0^2$. Here, M is the mass of the hole and v_0 is the (1D) velocity dispersion in the innermost halo just outside r_h. The precise profile for this DM density spike depends both on the properties of DM and the formation history of the SMBH. If the DM is collisionless with a cuspy, spherical, inner halo density obeying a generalized Navarro-Frenk-White (NFW) [1] profile then the density profile in the absence of the hole will follow a power law, $\rho(r) \sim r^{-\gamma_c}$. Simulations with DM alone yield typical values of $0.9 \lesssim \gamma_c \lesssim 1.2$ [2,3], but if baryons undergo dissipative collapse into the disk they can induce the adiabatic contraction of the central DM halo into a steeper power law [4–6], with values as high as $\gamma_c \sim 1.6$ allowed for the Milky Way [7].

If the SMBH grows adiabatically from a smaller seed [8] the SMBH then modifies the profile inside r_h, forming a DM spike within which $\rho(r) \sim r^{-\gamma_{\rm sp}}$, where $\gamma_{\rm sp} = (9 - 2\gamma_c)/(4 - \gamma_c)$ [9]. For $0 < \gamma_c \leq 2$ the power law $\gamma_{\rm sp}$ varies at most between 2.25 and 2.50 for this case. However, gravitational scattering off of a dense stellar component inside r_h could heat the DM, softening the spike profile and ultimately driving it to a final equilibrium value of $\gamma_{\rm sp} = 1.5$ [10–12], or even to disruption [13]. Other spikes, characterized by other power laws, are obtained from different formation histories for the BH within its host halo, such as the sudden formation of a SMBH through mergers or gradual growth from an inspiraling off-center seed [14], or in the presence of DM self-interactions [15], as reviewed in e.g. [16,17].

DM annihilations in the innermost region of the spike weaken the density profile there. For standard WIMP models, wherein the annihilation cross section $\langle\sigma v\rangle$ is a constant (i.e., s-wave annihilation) it was suggested [9] that an "annihilation plateau" would form at the central region of the spike, in which case the DM profile would be flat. Let $r = r_{\rm ann}$ be the radius at which the DM density in the spike reaches $\rho_{\rm ann}$, the annihilation plateau density. At this radius the annihilation time scale equals the Galaxy age T, so that

$$\rho_{\rm ann} = \frac{m_\chi}{\langle\sigma v\rangle T}. \tag{1}$$

Here m_χ is the DM particle mass.

Vasiliev [18] subsequently showed that an annihilation plateau arises only if all DM particles move in *strictly circular orbits* about the central black hole. He demonstrated that if the DM distribution function is *isotropic*, which he noted was likely, the density continues to rise with decreasing distance r from the black hole, forming a "weak cusp" and not a plateau. Within the weak cusp the density increases as $r^{-1/2}$ for s-wave annihilation. The reason is that particles in eccentric orbits with apocenters outside $r_{\rm ann}$ continue to contribute to the density inside $r_{\rm ann}$ and thereby maintain a weak inner cusp.

The distinction between an annihilation plateau and a weak cusp may have important observational consequences. Due to their extraordinarily high DM densities, BH-induced density spikes can appear as very bright gamma-ray point sources in models of annihilating DM [9–11,17,19–22]. Many of these models are now becoming detectable with the current and near-future high-energy

*Also at Department of Astronomy and NCSA, University of Illinois at Urbana-Champaign, Urbana, IL 61801.

gamma-ray experiments, and indeed the excess of $\sim 1-5$ GeV gamma rays from the inner few degrees of the Galactic Center (GC) observed by *Fermi* may prove to be a first signal of annihilating DM [23–25], although tension with limits from dwarf galaxies [26] and the statistical properties of the photons in the GC excess [27,28] may indicate an astrophysical explanation for the GC excess such as a new population of pulsars (see, e.g., [29–31]). In any case, self-annihilating DM within a spike can easily lead to gamma-ray point sources bright enough to be seen potentially by existing gamma-ray telescopes [17,22]. Now the dominant contribution to the annihilation signal from the spike comes from the region near $r_{\rm ann}$. This holds whether it originates from DM s-wave or from p-wave annihilations [17,22]. The magnitude of the signal thus depends on the density and velocity profiles in the region where the spike transitions to a weak cusp.

This result has not been fully appreciated, since it has not been incorporated into many recent applications. Consequently it seems worthwhile to revisit the issue. In general, a weak cusp of this form is obtained whenever DM initially following a power-law density profile attains sufficiently high densities that its self-annihilation becomes important. Thus in principle a weak cusp can form even in the absence of a spike, e.g. for a standard NFW cusp, $\gamma_c = 1$. In practice, given typical Galactic parameters and a thermal s-wave annihilation cross section, the DM density would only reach $\rho_{\rm ann}$ for radii very near the BH, rendering the weak cusp observationally insignificant. For p-wave annihilations, and for $\gamma_c \lesssim 1$, the weak cusp would not exist at all in this case.

We begin by providing a simple physical argument leading to analytic expressions for an isotropic phase space distribution function and resulting density and velocity dispersion profiles in a DM spike with a weak cusp. Our radial density profile for this case agrees with the result found by Vasiliev [18], who provided a scaling argument that also allows for an anisotropic initial spike. We next refine our analytic model by incorporating a loss-cone boundary condition that accounts for the direct capture of DM particles by the black hole, making the distribution anisotropic. Finally, we integrate the collisionless Boltzmann equation numerically, allowing for an anisotropic distribution function, and study how the weak cusp forms in the spike and grows with time. We again confirm the numerical results reported in [18] for s-wave annihilation but now we extend the analysis to include p-wave annihilation, with cross sections that vary as $\langle\sigma v\rangle \propto v^2(r)/c^2$, where $v(r)$ is the DM velocity dispersion and c the speed of light. We find that the annihilation cusp is even weaker (i.e. less steep) for p-wave than for s-wave annihilations, but it still is not a flat plateau.

In Sec. II we present our simple, pedagogic, analytic model for an isotropic DM spike with a weak cusp and in Sec. III we improve the model by including a capture loss cone, which induces an anisotropy. In Sec. IV we solve the Boltzmann equation directly and determine the time-dependent growth of the weak cusp, both for s-wave and p-wave DM annihilations. We adopt units with $G = 1 = c$ unless otherwise noted.

II. ISOTROPIC MODEL: $f = f(E)$

A. Density

An isotropic distribution function for a stationary distribution of collisionless matter of a single species is of the form $f = f(E)$, where E is the energy per unit mass of a particle. We adopt Newtonian gravitation and consider the energy of particles in orbit about the black hole:

$$E = \frac{1}{2}v^2 + \Phi(r), \qquad \Phi(r) = -\frac{M}{r}. \tag{2}$$

The mass density in the spike is obtained from the distribution function $f(E)$ according to

$$\begin{aligned}\rho(r) &= 4\pi \int v^2 f dv \\ &= 4\pi \int_{-M/r}^{0} \left[2\left(E + \frac{M}{r}\right)\right]^{1/2} f(E) dE.\end{aligned} \tag{3}$$

We will adopt the following simplification: let there be no surviving particles with orbits that reside entirely within $r_{\rm ann}$, while the particles whose orbits are either partly or entirely outside $r_{\rm ann}$ are described by the unperturbed spike distribution function. Thus we assume that all particles that orbit entirely within $r_{\rm ann}$ have been annihilated in the age of the Galaxy, while those which spent part or all of their time outside this radius have avoided annihilation altogether. Crudely, particles spend most of their time near apocenter, not pericenter, so they are more likely to survive whenever their orbits take them outside $r_{\rm ann}$. Mathematically, this assumption may be expressed as

$$\begin{aligned} f &= f(E), \qquad 0 \geq E \geq -M/r_{\rm ann}, \\ &= 0, \qquad E < -M/r_{\rm ann}. \end{aligned} \tag{4}$$

Inserting Eq. (4) into Eq. (3) yields

$$\rho(r) = 4\pi \int_{-\frac{M}{r}}^{0} \left[2\left(E + \frac{M}{r}\right)\right]^{1/2} f(E) dE, \quad r \geq r_{\rm ann}, \tag{5}$$

$$= 4\pi \int_{-\frac{M}{r_{\rm ann}}}^{0} \left[2\left(E + \frac{M}{r}\right)\right]^{1/2} f(E) dE, \qquad r < r_{\rm ann}. \tag{6}$$

By construction Eq. (5) gives the unperturbed spike profile for all $r \geq r_{\rm ann}$. Substituting the variable $y = -Er/M$ and adopting a power-law spike distribution function, $f(E) = K|E|^p$, where K is a (normalization) constant, we obtain

$$\rho(r) = 2^{5/2}\pi I_{1/2}(p;1)K\left(\frac{M}{r}\right)^{(p+3/2)} = \rho_{\rm ann}\left(\frac{r_{\rm ann}}{r}\right)^{(p+3/2)}, \qquad r \geq r_{\rm ann}, \tag{7}$$

where

$$I_{1/2}(p;q) \equiv \int_0^q (1-y)^{1/2} y^p dy, \tag{8}$$

and $I_{1/2}(p;1) = B(p+1,3/2)$, where $B(x,y)$ is the familiar beta function. For a power-law spike profile $\gamma_{\rm sp} = p + 3/2$.

Consider now the density profile for $r < r_{\rm ann}$ given by Eq. (6),

$$\rho(r) = 2^{5/2}\pi I_{1/2}\left(p;\frac{r}{r_{\rm ann}}\right)K\left(\frac{M}{r}\right)^{(p+3/2)} = \rho_{\rm ann}\frac{I_{1/2}(p;\frac{r}{r_{\rm ann}})}{I_{1/2}(p;1)}\left(\frac{r_{\rm ann}}{r}\right)^{(p+3/2)}, \qquad r < r_{\rm ann}. \tag{9}$$

Here $I_{1/2}(p;\frac{r}{r_{\rm ann}})/I_{1/2}(p;1) = B(p+1,3/2;\frac{r}{r_{\rm ann}})$, where $B(a,b;x)$ is the incomplete beta function. Evaluating the density for $r/r_{\rm ann} \ll 1$, noting $I_{1/2}(p,q) \approx q^{p+1}/(p+1)$ for $q \ll 1$, yields

$$\rho(r) \approx \frac{2^{5/2}\pi}{p+1}K\left(\frac{M}{r_{\rm ann}}\right)^{(p+1)}\left(\frac{M}{r}\right)^{1/2} = \frac{\rho_{\rm ann}}{(p+1)I_{1/2}(p;1)}\left(\frac{r_{\rm ann}}{r}\right)^{1/2}, \qquad r \ll r_{\rm ann}. \tag{10}$$

Equation (10) is exactly what we set out to prove: the density well inside $r_{\rm ann}$ scales like $r^{-1/2}$. Notice that this scaling behavior is independent of the power p. A continuous match between the inner and outer spike profiles can be obtained by numerically evaluating Eq. (9) and joining it to Eq. (7), which we do in Fig. 1.

In the absence of annihilation, the adiabatic spike that forms in a DM cluster initially characterized by a power-law density profile $\rho(r) \sim r^{-\gamma}$, $0 < \gamma < 2$, gives rise to a power-law profile with $2.25 < \gamma_{\rm sp} < 2.50$ [9]. The profiles when annihilation is incorporated are plotted in Fig. 1 for the limiting values of $\gamma_{\rm sp}$. A DM cluster that has an isothermal (and not a power-law) core initially forms an adiabatic spike with $\gamma_{\rm sp} = 1.5$ [8]. The spike profile for this value (which may also be reached if the DM spike is subsequently heated by scattering off stars [10,11]) is also shown in the figure, again allowing for annihilations.

It can be shown that the contribution of DM particles *unbound* to the BH, with energies $E = 3v_0^2/2 > 0$, also scales as $r^{-1/2}$ everywhere inside the BH zone of influence, i.e. $r \lesssim M/v_0^2$ [see [32], Eq. (14.2.22)]. However, their contribution inside $r_{\rm ann}$ is much smaller in magnitude than the contribution of (eccentric) bound particles, as the spike density of these contributing bound particles is much larger than unbound particles.

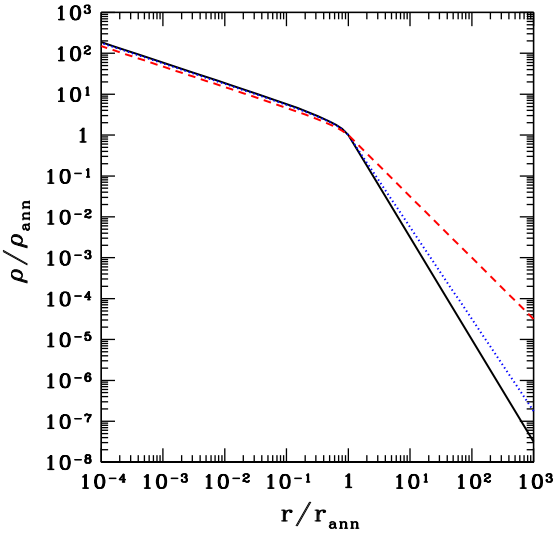

FIG. 1. DM density profile in an adiabatic spike around a black hole, allowing for annihilation. For $r \geq r_{\rm ann}$ the density varies as $r^{-\gamma_{\rm sp}}$, where $\gamma_{\rm sp} = 2.5$ (black solid line), 2.25 (blue dotted line) and 1.5 (red dashed line). For $r < r_{\rm ann}$ annihilations soften the spike to a weak cusp with $\rho(r) \sim r^{-1/2}$. Here ρ and r are normalized to their values at $r_{\rm ann}$.

We also note that at first glance there is nothing in the above argument that distinguishes s-wave from p-wave annihilation. The key point is that the time scale for annihilation decreases with decreasing r in a canonical spike. It is this feature that is reflected in Eq. (4) for the distribution function. This decrease is even more rapid as r decreases for p-wave than for s-wave annihilation, given the additional velocity dependence in the former case. So we again expect a weak cusp to form in the innermost region about the black hole. However, we note that in the case of p-wave annihilation the annihilation density $\rho_{\rm ann}$ given by Eq. (1) is not a constant but decreases with decreasing radius. For purely circular orbits we would then expect that instead of a flat plateau density profile inside $r_{\rm ann}$ we would have a density that decreases as r decreases. As the orbits in the cusp are dominated by highly eccentric and not circular orbits, the cusp will not exhibit this decrease. However, we do anticipate that the cusp profile for p-wave annihilations will be somewhat weaker (i.e. flatter) than for s-wave annihilations due to the decreasing value of $\rho_{\rm ann}$ with decreasing distance. This expectation is borne out by our solution to the Boltzmann equation in Sec. IV.

The canonical profiles for an adiabatic spike differ considerably from those arising in the case of self-interacting DM (SIDM), as shown in [15]. Moreover, the effects of annihilation are washed out for SIDM, as the distribution

function is constantly replenished inside $r_{\rm ann}$ by DM elastic scatterings. Hence there is no transition to a "weak cusp" inside the spike for SIDM.

Finally, we emphasize that Eq. (4) for the distribution function is only approximate. The true distribution function, though spherical, is not strictly isotropic and is better described by a function of the form $f(E,J)$, where J is the angular momentum per unit mass of a DM particle. To obtain the correct function an integration of the time-dependent Boltzmann equation with an annihilation sink term is required to determine $f(E,J;t)$. Vasiliev performed such an integration for s-wave annihilation. We will repeat the calculation in Sec. IV, incorporating a capture loss cone, and also do the calculation for p-wave annihilation.

B. Velocity dispersion

Now consider the (3D) velocity dispersion everywhere in the spike. It is obtained from

$$v^2(r) = \frac{4\pi}{\rho(r)}\int v^4 f dv = \frac{4\pi}{\rho(r)}\int_{-M/r}^{0}\left[2\left(E+\frac{M}{r}\right)\right]^{3/2} f(E)dE, \qquad (11)$$

which, when Eq. (4) is inserted, yields

$$v^2(r) = \frac{2^{7/2}\pi}{\rho(r)} K I_{3/2}(p;1)\left(\frac{M}{r}\right)^{p+5/2}, \qquad r \geq r_{\rm ann}, \qquad (12)$$

$$= \frac{2^{7/2}\pi}{\rho(r)} K I_{3/2}\left(p;\frac{r}{r_{\rm ann}}\right)\left(\frac{M}{r}\right)^{p+5/2}, \qquad r < r_{\rm ann}. \qquad (13)$$

Here

$$I_{3/2}(p;q) \equiv \int_0^q (1-y)^{3/2} y^p dy, \qquad (14)$$

where $I_{3/2}(p;1) = B(p+1,5/2)$ and where $I_{3/2}(p;r/r_{\rm ann})/I_{3/2}(p;1) = B(p+1,5/2;r/r_{\rm ann})$. Evaluating Eqs. (12) and (13), using Eqs. (7), (9) and (10) for $n(r)$, yields

$$v^2(r) = \frac{3}{p+5/2}\frac{M}{r}, \qquad r \geq r_{\rm ann}, \qquad (15)$$

$$= 2\frac{I_{3/2}(p;r/r_{\rm ann})}{I_{1/2}(p;r/r_{\rm ann})}\left(\frac{M}{r}\right), \qquad r < r_{\rm ann}, \qquad (16)$$

and

$$v^2(r) \approx 2\frac{M}{r}, \qquad r \ll r_{\rm ann}. \qquad (17)$$

The corresponding values for the 1D velocity dispersion $v_{\hat{i}}^2(r) = v^2(r)/3$, $\hat{i} = \{\hat{r},\hat{\theta},\hat{\phi}\}$, are

$$v_{\hat{i}}^2(r) = \frac{1}{p+5/2}\frac{M}{r}, \qquad r \geq r_{\rm ann}, \qquad (18)$$

$$= \frac{2}{3}\frac{I_{3/2}(p;r/r_{\rm ann})}{I_{1/2}(p;r/r_{\rm ann})}\left(\frac{M}{r}\right), \qquad r < r_{\rm ann}, \qquad (19)$$

and

$$v_{\hat{i}}^2(r) \approx \frac{2}{3}\frac{M}{r}, \qquad r \ll r_{\rm ann}. \qquad (20)$$

Hence in both power-law regimes, with $\rho(r) \sim r^{-\beta}$, where $\beta = p + 3/2$ for $r \geq r_{\rm ann}$ and $\beta = 1/2$ for $r \ll r_{\rm ann}$, we find $v_{\hat{i}}^2(r) = v^2(r)/3 = \frac{M}{r}\frac{1}{1+\beta}$, as assumed in [17]. A continuous transition between the inner and outer spike is obtained by evaluating Eq. (13) numerically for $0 < r/r_{\rm ann} < 1$. We do this in Fig. 2 for the profiles shown in Fig. 1.

Finally, we note that the above results should apply well to p-wave as well as s-wave annihilations, allowing for the smaller value of $r_{\rm ann}$ and the slight decrease in β in the weak cusp for p-wave annihilations (from $\beta = 0.5$ to $\beta \approx 0.34$; see Sec. IV).

III. LOSS CONE: $f = f(E, J)$

We now incorporate a realistic inner boundary condition that all particles that *ever* reach inside $r_{\rm bh} = 4M$ are captured by the black hole within a single orbital period. As a result, since DM is assumed collisionless (except for annihilations), those capture orbits are never replenished and the distribution function vanishes for these trajectories. Here we take $r_{\rm bh}$ to be the radius of marginally bound circular orbits and the minimum periastron of all parabolic orbits about a Schwarzschild black hole [15,32,33]. This capture constraint induces a loss cone in phase space: for any particle of energy E, there are no particle orbits with angular momentum per unit mass satisfying $J \leq J_{\rm loss}(E)$, where $J_{\rm loss}(E)$ is the angular momentum at which $r_p(E, J_{\rm loss}) = r_{\rm bh}$. Here $r_p(E,J)$ is the pericenter radius of bound particles of energy E and angular momentum J in (elliptical) orbit about the black hole. Accordingly, we have

$$J_{\rm loss}(E) = r_{\rm bh}\left[2\left(E+\frac{M}{r_{\rm bh}}\right)\right]. \qquad (21)$$

Following [18], we change phase-space variables from $\{E,J\}$ to $\{E,R\}$, defining $R \equiv J^2/J_c^2$, where $J_c = M/(-2E)^{1/2}$ is the angular momentum of a circular orbit of energy E. Hence $0 \leq R \leq 1$. Equation (21) then gives

$$R_{\rm loss}(E) = 4\frac{r_{\rm bh}}{M}\left(|E|(1-|E|\frac{r_{\rm bh}}{M}\right), \qquad 0 \geq E \geq -\frac{M}{(2r_{\rm bh})}. \qquad (22)$$

Orbits with $E < -M/(2r_{\rm bh})$ cannot avoid penetrating the inner boundary at $r_{\rm bh}$ and hence do not survive capture. Annihilations thus are relevant only when $r_{\rm ann} > 2r_{\rm bh}$. Incorporating the loss-cone boundary condition in our simple distribution function that accounts for annihilations when $r_{\rm ann} > 2r_{\rm bh}$ yields a two-dimensional distribution function,

$$f_{\rm loss}(E,R) = f(E), \qquad 0 \geq E \geq -\frac{M}{r_{\rm ann}} \quad \text{and} \quad R \geq R_{\rm loss}(E),$$
$$= 0, \qquad E < -\frac{M}{r_{\rm ann}} \quad \text{or} \quad R < R_{\rm loss}(E). \tag{23}$$

The above form guarantees that $f_{\rm loss}(E,R) = 0$ for all $E < -M/(2r_{\rm bh})$. Strictly a function of the integrals of motion E and J (or E and R), $f_{\rm loss}(E,R)$ is a steady-state solution of the collisionless Boltzmann equation, according to the Jeans theorem.

Obtaining the density and velocity dispersion profiles generated by this distribution function requires a two-dimensional integration over velocity space inside the spike. Using the expression

$$d^3v = \frac{2\pi J_c^2 dR dE}{r^2 |v_{\hat{r}}|}, \tag{24}$$

where $v_{\hat{r}}$ is the radial velocity, we determine these moments according to

$$\rho(r) = 2^{-1/2}\pi\left(\frac{M}{r}\right)^{3/2} \times \int_0^1 \frac{d\varepsilon}{\varepsilon}\int_0^{4\varepsilon(1-\varepsilon)} dR f_{\rm loss}\left(-\frac{\varepsilon}{r}, R\right)\frac{1}{\sqrt{1-\varepsilon-\frac{R}{4\varepsilon}}}, \tag{25}$$

$$\rho v^2(r) = 2^{1/2}\pi\left(\frac{M}{r}\right)^{5/2} \times \int_0^1 \frac{d\varepsilon(1-\varepsilon)}{\varepsilon}\int_0^{4\varepsilon(1-\varepsilon)} dR f_{\rm loss}\left(-\frac{\varepsilon}{r}, R\right)\frac{1}{\sqrt{1-\varepsilon-\frac{R}{4\varepsilon}}}, \tag{26}$$

where $\varepsilon \equiv -Er/M$.

The results of the integrations are shown in Fig. 3 for density profiles and Fig. 4 for the velocity profiles. Shown are curves for the same power-law spikes $f(E) = K|E|^p$ plotted in Figs. 1 and 2, but now clipped in R in accord with Eq. (23). Here we normalize radii to a fiducial outer spike radius r_0, where the density is assumed to be ρ_0. We fix the annihilation radius at $r_{\rm ann}/r_0 = 2.2 \times 10^{-3}$ and the capture radius at $r_{\rm bh}/r_0 = 5 \times 10^{-8}$. As we will see in the next section, if we assign r_0 to reside near the outer radius of the DM spike, where the particles bound to the black hole join on to the ambient nuclear core, then these dimensionless ratios are within an order of magnitude of those inferred for the DM spike in the Milky Way. In this case $r_0 \approx M/v_0^2$, where v_0 is the velocity dispersion characterizing the nuclear core and M is the mass of Sgr A*. We postpone making a more careful match to realistic Milky Way parameters to the next section.

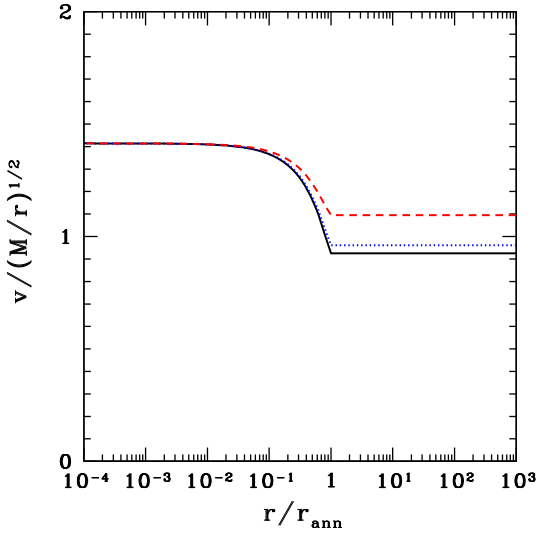

FIG. 2. DM velocity dispersion (3D) in an adiabatic spike around a black hole, allowing for annihilation. Curves are labeled as in Fig. 1. Here v is normalized to $(M/r)^{1/2}$, where M is the mass of the black hole.

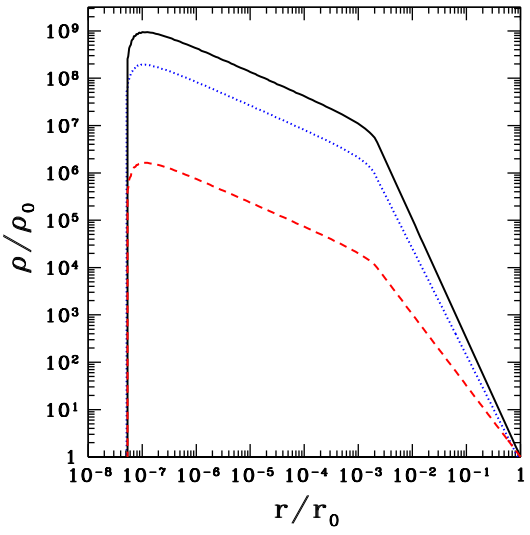

FIG. 3. DM density profile in an adiabatic DM spike around a black hole, allowing for annihilation and black hole capture. Curves are labeled as in Fig. 1. The densities and radii are normalized to their values at fiducial radius r_0 in the outer spike. The annihilation radius is fixed at $r_{\rm ann}/r_0 = 2.2 \times 10^{-3}$ and the capture radius at $r_{\rm bh}/r_0 = 5 \times 10^{-8}$.

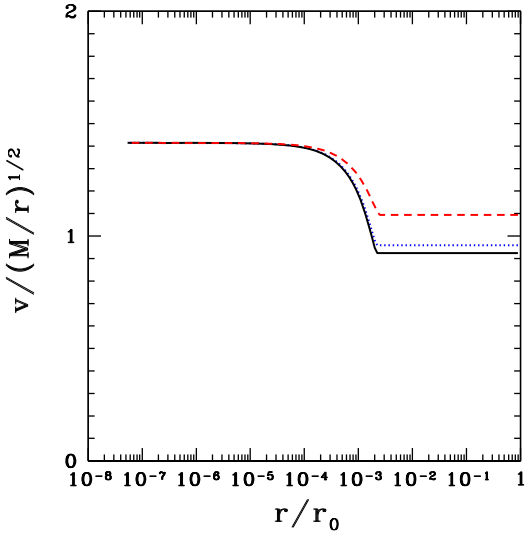

FIG. 4. DM velocity dispersion (3D) in an adiabatic DM spike around a black hole, allowing for annihilation and black hole capture. Curves are labeled and parameters assigned as in Fig. 3. Here v is normalized to $(M/r)^{1/2}$.

As is intuitive, the above density profiles differ little from those found in the absence of a loss-cone boundary condition, except at radii approaching $r_{\rm bh}$, where the loss cone grows to occupy an appreciable fraction of phase space. For $r_{\rm bh} \lesssim r \ll r_{\rm ann}$ we again find $n(r) \sim r^{-1/2}$. The magnitude of the 3D velocity dispersion remains fairly insensitive to the presence of the loss cone, but the eccentric orbits, which dominate the weak cusp, are also destroyed as $r \to r_{\rm bh}$.

IV. EVOLUTION: $f(E, R; t)$

We now consider the evolution with time of the DM profile in the spike by integrating the Boltzmann equation directly, allowing for annihilation. We adopt the approach in [18], but now we incorporate a loss-cone boundary condition in $f(E, R; t)$ and treat two cases: one for s-wave and the other for p-wave annihilation. We again assume that the black hole grew to its present mass M adiabatically at the center of the inner, spherical, DM Galactic halo, where the density profile was $\rho(r) \sim r^{-\gamma_c}$, and that this growth occurred over a time $t \ll T = 10^{10}$ yr. The result is the formation of a DM spike about the black hole that obeys a new power-law density profile $\rho(r) \sim r^{-\gamma_{sp}}$, with $\gamma_{sp} = (9 - 2\gamma_c)/(4 - \gamma_c)$ [9], corresponding to a power-law phase-space distribution function $f(E) \propto |E|^p$ with $p = \gamma_{sp} - 3/2$.

We specialize to parameters appropriate to the Milky Way nucleus and typical WIMP particle models, which is the basis of the "canonical" adiabatic spike in [17,22]. We recall that $\gamma_c = 1$ is the standard NFW value for the central DM halo. Following [17] we take instead $\gamma_c = 1.26$, the best-fit value reported in [23], which provides a recent analysis of the *Fermi* data of the $\sim 1 - 3$ GeV gamma-ray excess from the Galactic center and the possibility that it might be a signal of DM annihilations. This value then yields $\gamma_{sp} = 2.36$ and $p = 0.86$ for an adiabatic spike.

The outer boundary of the spike is taken to be at $r_b = 0.2 r_h = 0.34$ pc, where $r_h = M/v_0^2$, $M = 4 \times 10^6\ {\rm M}_\odot$ [34,35] and $v0 = 105$ kms^{-1} [36]. The inner boundary is at $r_{\rm bh} = 6 \times 10^6$ km. From the DM density in the solar neighborhood, $\rho_D = 0.008\ {\rm M}_\odot\ {\rm pc}^{-3}$ [37] at a distance $D = 8.5$ kpc from the Galactic center [23], we infer the DM density at r_b to be $\rho_b = \rho_D (D/r_b)^{\gamma_c} = 2.8 \times 10^3\ {\rm M}_\odot\ {\rm pc}^{-3}$.

The DM annihilation cross sections are given by

$$\langle \sigma v \rangle = \langle \sigma v \rangle_{\rm can} \left(\frac{v^2}{v_{\rm fo}^2} \right)^s \tag{27}$$

where $s = 0$ for s-wave annihilation and $s = 1$ for p-wave annihilation. Here we follow [17,23] and take $\langle \sigma v \rangle_{\rm can} = 1.7 \times 10^{-26}\ {\rm cm}^3\ {\rm s}^{-1}$, close to the value expected for a thermal relic origin of DM, with the freeze-out parameter $v_{\rm fo} = c/4$ for $s = 1$. For the DM mass we choose $m_\chi = 35$ GeV.

Given the above particle models we calculate that at $t = T = 10^{10}$ yr the annihilation plateau densities defined by Eq. (1) in the DM spike are $\rho_{\rm ann}(s\text{-wave}) = 1.7 \times 10^8\ {\rm M}_\odot\ {\rm pc}^{-3}$ and $\rho_{\rm ann}(p\text{-wave}) = 6.6 \times 10^{10}\ {\rm M}_\odot\ {\rm pc}^{-3}$. These densities are reached at radii $r_{\rm ann}(s\text{-wave}) = 3.1 \times 10^{-3}$ pc and $r_{\rm ann}(p\text{-wave}) = 2.5 \times 10^{-4}$ pc in the spike, within which we expect the density spike to transition to a weak cusp. The cusp is smaller for p-wave than for s-wave annihilation since the annihilation cross section is reduced by $\sim v^2/c^2$, so the time scale for p-wave annihilation to destroy matter in the innermost spike is correspondingly longer.

The Boltzmann equation may be written as

$$\frac{\partial f(\mathbf{r}, \mathbf{v}; t)}{\partial t} = -\frac{\rho(\mathbf{r})}{m_\chi} \langle \sigma v \rangle f(\mathbf{r}, \mathbf{v}; t), \tag{28}$$

which can be transformed to yield

$$\frac{\partial f(E, R; t)}{\partial t} = -\frac{\overline{\rho \langle \sigma v \rangle}}{m_\chi} f(E, R; t), \tag{29}$$

or

$$\frac{\partial f(E, R; \tau)}{\partial \tau} = -\frac{\overline{\rho v^{2s}}}{\rho_{\rm a} v_{\rm fo}^{2s}} f(E, R; \tau). \tag{30}$$

Here $\tau = t/T$, ρ_a is given by Eq. (1) for $s = 0$, and is thus a constant, and the overbar denotes a radial average over orbital period $P(E)$,

$$\overline{\rho v^{2s}} = \frac{1}{P(E)} \oint \rho(r) v^{2s}(r) \frac{dr}{v_{\hat{r}}} = \int_{1-\sqrt{1-R}}^{1+\sqrt{1-R}} \rho(x r_c) v^{2s}(x r_c) \frac{dx}{\pi \sqrt{2/x - 1 - R/x^2}}. \tag{31}$$

In writing Eq. (31) we set $r = x r_c$, where $r_c = M/(-2E)$ is the radius of a circular orbit with energy E. The profiles for ρ and v appearing in the integrands in Eq. (31) are obtained at time τ from Eq. (25), with $f_{\rm loss}(E,R)$ replaced by the current value of $f(E,R;\tau)$. Loss-cone boundary conditions are imposed throughout the evolution. We take as initial data an adiabatic distribution function specified by Eq. (23), with $f(E) = K|E|^p$, $p = 0.86$ and $r_{\rm ann} = 0$ (i.e., no annihilation imprint at $\tau = 0$).

We integrate the evolution Eq. (30) by finite differencing in E and R and evolving in time τ by a first-order semi-implicit method. All time integrations and phase-space quadratures are repeated with finer resolution to check reliability. Results for the density and velocity profiles are summarized in Figs. (5) and (6), respectively.

The s-wave profile in Fig. (5) exhibits a weak cusp inside the annihilation region at each time, within which the density varies as $r^{-1/2}$. This result is in accord with our simplified models constructed in Secs. II and III. As $\rho_{\rm ann}$ decreases with time, the weak cusp grows, eating its way outward into the steeper spike. The p-wave profile behaves qualitatively similarly, with two notable differences. The first is that for the same evolution time the p-wave cusp is smaller, as described above. The second is that the p-wave cusp is somewhat shallower, varying as $r^{-0.34}$ rather than $r^{-1/2}$. This may be understood by noting that the annihilation plateau density $\rho_{\rm ann}$ given by Eq. (1) decreases with decreasing distance from the black hole, since the velocity dispersion and annihilation cross section increase. Hence while the cusp is still filled with high eccentricity particles from outside the cusp that plunge inside at the pericenter, the lower eccentricity particles in the cusp are driven to lower ("plateau") densities the closer they are to the black hole. This effect causes the overall slope of the density profile in the cusp to fall slightly below 1/2 to ∼0.34 by $t = 10^{10}$ yr.

The velocity profiles plotted in Fig. 6 also show that the cusps grow in size with time and at any one time are larger for s-wave annihilation than for p-wave annihilation. Otherwise the profiles are identical in the unperturbed spike regions and very close in the cusp regions, conforming to those found for the simplified models in Secs. II and III.

Next we consider the luminosity profiles arising from DM annihilation within the spike. The photon luminosity emerging from radius r is given by

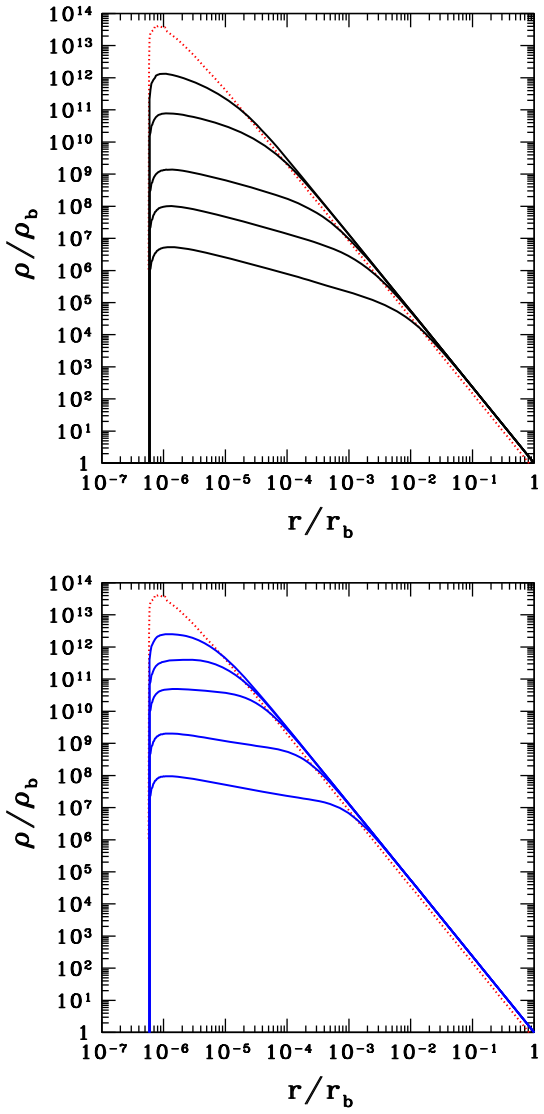

FIG. 5. Evolution of the density profile in a DM spike around Sgr A*, allowing for s-wave (top) and p-wave (bottom) annihilation and black hole capture. The dotted curve shows the initial adiabatic profile at $t = 0$. Moving downward, successive solid curves show the profiles at $t/T = 1.6 \times 10^{-7}, 4.8 \times 10^{-6}, 8.2 \times 10^{-4}, 2.4 \times 10^{-2}$ and 1.0 (top) and at $t/T = 4.9 \times 10^{-8}, 7.6 \times 10^{-7}, 2.0 \times 10^{-5}, 5.1 \times 10^{-3}$ and 1.0 (bottom), where $T = 10^{10}$ yr. The densities and radii are normalized to their values near the spike outer boundary at $r_b = 0.34$ pc, where $\rho_b = 2.8 \times 10^3\ {\rm M}_\odot\ {\rm pc}^{-3}$.

$$L(r) = \int_{r_{\rm bh}}^{r} \frac{1}{2} \frac{\rho(r)^2}{m_\chi^2} (2\epsilon_\gamma m_\chi) \langle \sigma v \rangle 4\pi r^2 dr, \tag{32}$$

where ϵ_γ is the fraction of the annihilation energy that goes into photons. The region between r and $2r$ that contributes most of the luminosity is centered near the peak of the function $dL(r)/dln(r)$, where according to Eqs. (27) and (32),

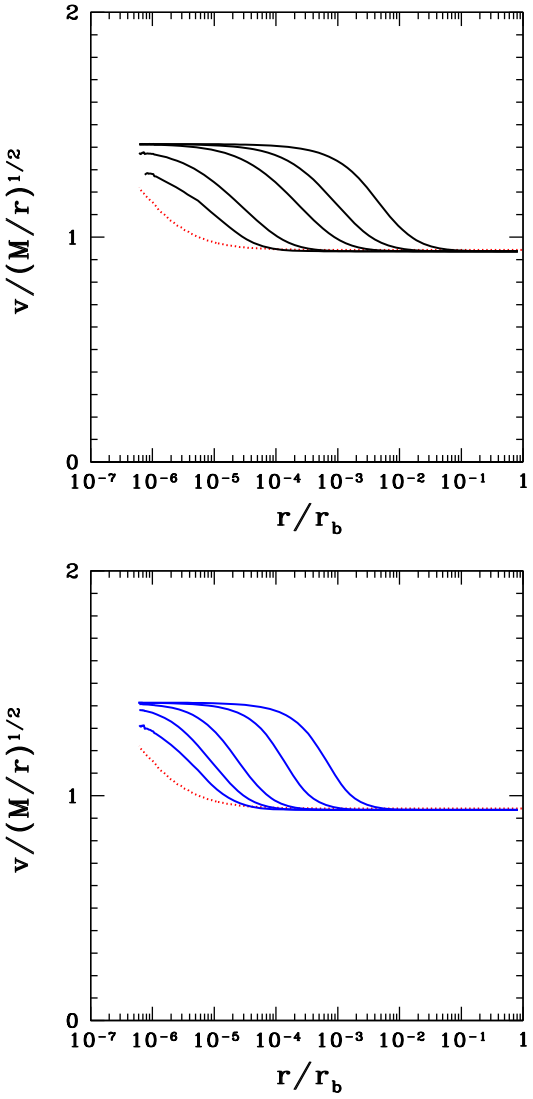

FIG. 6. Evolution of the velocity dispersion (3D) in a DM spike around Sgr A*, allowing for s-wave (top) and p-wave (bottom) annihilation and black hole capture. The dotted curve shows the initial adiabatic profile at $t = 0$. Moving upward, successive solid curves show the profiles at $t/T = 1.6 \times 10^{-7}, 4.8 \times 10^{-6}, 8.2 \times 10^{-4}, 2.4 \times 10^{-2}$ and 1.0 (top), and at $t/T = 4.9 \times 10^{-8}, 7.6 \times 10^{-7}, 2.0 \times 10^{-5}, 5.1 \times 10^{-3}$ and 1.0 (bottom), where $T = 10^{10}$ yr. Radii are normalized to the value near the spike outer boundary at $r_b = 0.34$ pc, and velocities are normalized to $(M/r)^{1/2}$.

$$\frac{dL(r)}{dln(r)} \propto r^3 \rho^2 \left(\frac{v^2(r)}{v_{\rm fo}^2}\right)^s. \tag{33}$$

This function is plotted in Fig. 7 for the two cases, along with the corresponding density profiles. Results are shown for both the initial spike and the spike at $t = T = 10^{10}$ yr. Several features are evident from the plot. The first is that for both s-wave and p-wave annihilation the dominant emission originates from the innermost region of the spike near $r \gtrsim r_{\rm bh}$ initially, but moves out to the outer edge of the

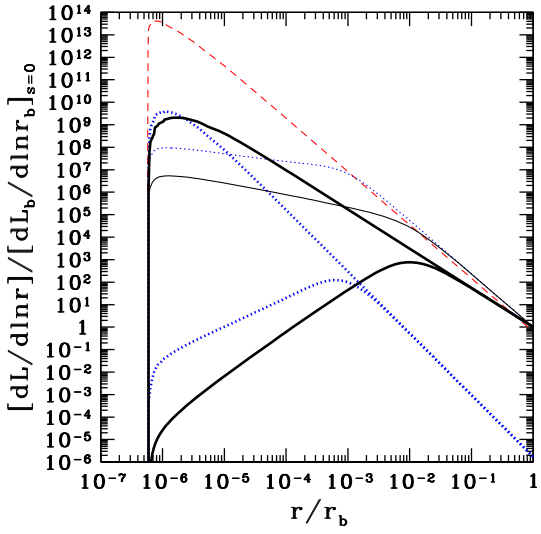

FIG. 7. The luminosity profile from annihilation in a DM spike around Sgr A*. The heavy solid (black) curves show the luminosity for s-wave annihilation at $t = 0$ (upper) and at $t = 10^{10}$ yr (lower). The heavy dotted (blue) curves show the luminosity for p-wave annihilation at $t = 0$ (upper) and at $t = 10^{10}$ yr (lower). For comparison, the dashed (red) curve shows the DM adiabatic density profile at $t = 0$, while the density profile at $t = 10^{10}$ yr is shown for s-wave annihilation by the thin solid (black) curve and for p-wave annihilations by the thin dotted (blue) curve. All luminosities are normalized by the initial s-wave luminosity at the spike outer boundary at $r_b = 0.34$ pc. All radii are normalized by r_b.

weak cusp $r \sim r_{\rm ann}$ at later times. As annihilations eat their way further into the spike and $r_{\rm ann}$ moves outward with time, the magnitude of the luminosity falls. Apart from the initial time, when the luminosities are comparable, the luminosity is greater for s-wave annihilation than for p-wave annihilation. This difference results from the fact that the main radiating region around $r_{\rm ann}$ has a much smaller volume and the cross section has an additional factor of v^2/c^2 for p-wave versus s-wave annihilation.

We note that for a flat plateau instead of a weak cusp the luminosity profile plotted in Fig. 7 would plummet faster for all $r < r_{\rm ann}$ and thereby reduce the overall annihilation flux. For the Galactic parameters adopted here it is a $\sim$10% reduction for s-wave annihilation and less for p-wave annihilation, but can be larger for different parameters or DM halos.

Figure 7 shows that most of the luminosity from the spike originates from the region around $r_{\rm ann}$ and that $r_{\rm ann} \gg M$ at $t = 10^{10}$ yr. As a result, our Newtonian analysis of the bulk profiles in this region and, hence, the annihilation luminosity, are little modified by relativistic corrections. However, it has been suggested that a high-energy tail in the (gamma-ray) spectrum might arise from the Penrose process in the vicinity of a rapidly spinning Kerr black hole [38]. Here a fully relativistic treatment is necessary, but the

ambient spike and weak cusp should be close to the profiles obtained here for all $r \gg M$.

V. SUMMARY

We have reinvestigated the effect of DM self-annihilations on the distribution of collisionless DM in a spherical density spike around a BH. These spikes can reach the so-called "annihilation plateau" density $\rho_{\rm ann} = m_\chi/(\langle\sigma v\rangle T)$ at a radius $r = r_{\rm ann}$, where the time scale for DM annihilation becomes equal to the age of the Galaxy. Interior to this radius, DM annihilations are important for determining the radial density and velocity dispersion profiles of DM, with potentially observable consequences for indirect detection. We revisit and extend the results of [18] for s-wave annihilation cross sections, and provide the first results for nonconstant annihilation cross sections, with the very well-motivated case of p-wave annihilations.

We first give a simple physical argument for the case of an isotropic phase space distribution function that yields analytic expressions for the DM density and velocity dispersion profiles within a DM spike with a weak cusp. This argument reproduces the result of [18] for the DM density profile in the case of a velocity-independent s-wave annihilation cross section, where the density follows a power law $\rho(r) \propto r^{-1/2}$ for radii below $r_{\rm ann}$. We then extend this analytic model to incorporate the direct capture of DM particles by the BH via a loss-cone boundary condition, making the resulting distribution anisotropic. Finally, to provide a full description of the (spherically symmetric) system, we integrate the collisionless Boltzmann equation numerically and study the formation of the weak cusp and its subsequent evolution with time. We find that the increasing annihilation cross section at decreasing radii in the case of p-wave annihilations flattens the annihilation cusp relative to that obtained with s-wave annihilations, yielding $\rho(r) \propto r^{-0.34}$ for the Galactic parameters adopted here, but still yields a cusp.

ACKNOWLEDGMENTS

It is a pleasure to thank B. Fields for helpful discussions. This paper was supported in part by NSF Grant No. PHY-1300903 and NASA Grant No. NN13AH44G at the University of Illinois at Urbana-Champaign.

[1] J. F. Navarro, C. S. Frenk, and S. D. M. White, Astrophys. J. **490**, 493 (1997).
[2] J. Diemand, M. Kuhlen, P. Madau, M. Zemp, B. Moore, D. Potter, and J. Stadel, Nature (London) **454**, 735 (2008).
[3] J. F. Navarro, A. Ludlow, V. Springel, J. Wang, M. Vogelsberger, S. D. M. White, A. Jenkins, C. S. Frenk, and A. Helmi, Mon. Not. R. Astron. Soc. **402**, 21 (2010).
[4] G. R. Blumenthal, S. M. Faber, R. Flores, and J. R. Primack, Astrophys. J. **301**, 27 (1986).
[5] O. Y. Gnedin, A. V. Kravtsov, A. A. Klypin, and D. Nagai, Astrophys. J. **616**, 16 (2004).
[6] M. Gustafsson, M. Fairbairn, and J. Sommer-Larsen, Phys. Rev. D **74**, 123522 (2006).
[7] M. Pato, F. Iocco, and G. Bertone, J. Cosmol. Astropart. Phys. 12 (2015) 001.
[8] P. J. E. Peebles, Gen. Relativ. Gravit. **3**, 63 (1972).
[9] P. Gondolo and J. Silk, Phys. Rev. Lett. **83**, 1719 (1999).
[10] D. Merritt, Phys. Rev. Lett. **92**, 201304 (2004).
[11] O. Y. Gnedin and J. R. Primack, Phys. Rev. Lett. **93**, 061302 (2004).
[12] D. Merritt, S. Harfst, and G. Bertone, Phys. Rev. D **75**, 043517 (2007).
[13] M. Wanders, G. Bertone, M. Volonteri, and C. Weniger, J. Cosmol. Astropart. Phys. 4 (2015) 004.
[14] P. Ullio, H. Zhao, and M. Kamionkowski, Phys. Rev. D **64**, 043504 (2001).
[15] S. L. Shapiro and V. Paschalidis, Phys. Rev. D **89**, 023506 (2014).
[16] M. Fornasa and G. Bertone, Int. J. Mod. Phys. D **17**, 1125 (2008).
[17] B. D. Fields, S. L. Shapiro, and J. Shelton, Phys. Rev. Lett. **113**, 151302 (2014).
[18] E. Vasiliev, Phys. Rev. D **76**, 103532 (2007).
[19] G. A. X., S. Profumo, and F. S. Queiroz, Phys. Rev. D **90**, 103508 (2014).
[20] A. Belikov and J. Silk, Phys. Rev. D **89**, 043520 (2014).
[21] T. Lacroix, C. Boehm, and J. Silk, Phys. Rev. D **92**, 043510 (2015).
[22] J. Shelton, S. L. Shapiro, and B. D. Fields, Phys. Rev. Lett. **115**, 231302 (2015).
[23] T. Daylan, D. P. Finkbeiner, D. Hooper, T. Linden, S. K. N. Portillo, N. L. Rodd, and T. R. Slatyer, Phys. Dark Univ. **12**, 1 (2016).
[24] F. Calore, I. Cholis, and C. Weniger, J. Cosmol. Astropart. Phys. 03 (2015) 038.
[25] M. Ajello *et al.* (Fermi-LAT Collaboration), Astrophys. J. **819**, 44 (2016).
[26] M. Ackermann *et al.* (Fermi-LAT Collaboration), Phys. Rev. Lett. **115**, 231301 (2015).
[27] S. K. Lee, M. Lisanti, B. R. Safdi, T. R. Slatyer, and W. Xue, Phys. Rev. Lett. **116**, 051103 (2016).
[28] R. Bartels, S. Krishnamurthy, and C. Weniger, Phys. Rev. Lett. **116**, 051102 (2016).
[29] K. N. Abazajian, N. Canac, S. Horiuchi, and M. Kaplinghat, Phys. Rev. D **90**, 023526 (2014).
[30] T. D. Brandt and B. Kocsis, Astrophys. J. **812**, 15 (2015).
[31] R. M. O'Leary, M. D. Kistler, M. Kerr, and J. Dexter, arXiv:1601.05797.

[32] S. L. Shapiro and S. A. Teukolsky, *Black Holes, White Dwarfs, and Neutron Stars: The Physics of Compact Objects* (New York, Wiley, 1983).
[33] L. Sadeghian, F. Ferrer, and C. M. Will, Phys. Rev. D **88**, 063522 (2013).
[34] A. M. Ghez, S. Salim, N. N. Weinberg, J. R. Lu, T. Do, J. K. Dunn, K. Matthews, M. R. Morris, S. Yelda, E. E. Becklin, T. Kremenek, M. Milosavljevic, and J. Naiman, Astrophys. J. **689**, 1044 (2008).
[35] R. Genzel, F. Eisenhauer, and S. Gillessen, Rev. Mod. Phys. **82**, 3121 (2010).
[36] K. Gültekin, D. O. Richstone, K. Gebhardt, T. R. Lauer, S. Tremaine, M. C. Aller, R. Bender, A. Dressler, S. M. Faber, A. V. Filippenko, R. Green, L. C. Ho, J. Kormendy, J. Magorrian, J. Pinkney, and C. Siopis, Astrophys. J. **698**, 198 (2009).
[37] J. Bovy and S. Tremaine, Astrophys. J. **756**, 89 (2012).
[38] J. D. Schnittman, Astrophys. J. **806**, 264 (2015).